RSC Advances

ROYAL SOCIETY OF CHEMISTRY

www.rsc.org/advances

Journal Name

ARTICLE

Discovery and Identification of Cdc37-Derived Peptides Targeting Hsp90-Cdc37 Protein-Protein Interaction

Lei Wang [a,b], Qi-Chao Bao [a,b], Xiao-Li Xu [a,b,c], Fen Jiang [a,b], Kai Gu [a,b], Zheng-Yu Jiang [a,b], Xiao-Jin Zhang [a,b,d], Xiao-Ke Guo [a,b,c], Qi-Dong You [a,b,*] and Hao-Peng Sun [a,b,c,*]

As an attractive anticancer target, Hsp90 chaperone machine regulates a wide range of oncoproteins. Most of Hsp90 inhibitors in clinical trials employ the same ATP blockage mechanism while little progress has been achieved in Hsp90-cochaperone complex. Numerous protein kinases associate with Hsp90-Cdc37 PPI, a potential target for treatment of cancers, to implement folding and maturation. In order to explore the key residues of Hsp90-Cdc37 binding interface for further design of peptide inhibitors, a combined strategy of molecular dynamics simulation and MM-PBSA analysis was performed. Subsequent design and identification of an eleven-residue peptide (**Pep-1**) directly derived from Cdc37 binding interface was achieved to exhibit 6.9 μM binding capacity and 3.0 μM ATPase inhibitory rate. This is the first evidence that a peptide inhibitor not only interferes with Hsp90 ATPase ability but also disrupts Cdc37-Hsp90 PPI.

1. Introduction

90-kDa heat-shock proteins (Hsp90) is a well-known target to interact with diverse client proteins including kinases, transcription factors and other structurally unrelated proteins. Over the past several years, global analysis of Hsp90 had made it a crucial target associated with more than 200 proteins.[1] The traditional pattern for Hsp90 inhibition is the blockade of ATP binding site, leading to many kinds of inhibitors in clinical trials such as geldanamycin analogues, purine-scaffold inhibitors, resorcinol derivatives and benzamides analogues.[2] However, as a weak ATPase, Hsp90's function relies on the ATP binding and hydrolyzing to produce energy. Most of the known Hsp90 inhibitors, targeting N-terminal ATP binding domain with similar binding capacity, show poor specificity leading to overt toxicity.[3] Up to now, none of them has reached the market.

Hsp90 works not only depending on ATP cycle but also requiring a complicated co-chaperones system.[4] Halting the formation of Hsp90 and its co-chaperones complex at various stages is also likely to achieve Hsp90 inhibition. Cell cycle division protein 37 (Cdc37), also known as p50, is one of the most important co-chaperones.[5]

a Jiangsu Key Laboratory of Drug Design and Optimization, China Pharmaceutical University, Nanjing, 210009, China
b State Key Laboratory of Natural Medicines, China Pharmaceutical University, Nanjing 210009, China
c Department of Medicinal Chemistry, School of Pharmacy, China Pharmaceutical University, Nanjing, 210009, China
d Department of Organic Chemistry, School of Science, China Pharmaceutical University, Nanjing, 210009, China

*Corresponding authors. China Pharmaceutical University, Nanjing 210009, China
E-mail addresses: sunhaopeng@163.com (H. Sun), youqidong@gmail.com (Q. You).

Most client proteins of Hsp90 need Cdc37 to mediate their maturation. A lot of protein kinases (such as BRAF,[6] P38α,[7] SGK3,[8] PKC,[9] KIT,[10] IKKβ,[11] Rho,[12] CDK4,[13] ERK5,[14] c-Src,[15] IRE1α,[16] CDK2,[17] TDP43,[18] IRAK1,[19] Tau,[20] AKT,[21] UIK1,[22] LKB1[23]) whose biological function relies on the protein-protein interaction (PPI) of Hsp90-Cdc37 complex have been widely reported in recent years. Silencing of Cdc37 disrupts the association between Hsp90 and kinase clients, thus inducing proteasome dependent degradation.[24] A natural product, celastrol, has been identified to disrupt the Hsp90-Cdc37 complex in cancer cells. This discovery supported that the strategy targeting the PPI of Hsp90-Cdc37 was feasible.[25] As there is no cocrystal structure available, the binding site of celastrol to Hsp90-Cdc37 complex is still unclear so far. However, three potential binding sites have been discussed, including Hsp90 N-terminal,[25] Hsp90 C-terminal[26] or covalently bound to Cdc37 middle domain[27]. Although celastrol shows moderate inhibitory effect on Hsp90-Cdc37 complex, lack of selectivity, poor binding capacity and difficulty in structural modification restrict its further development. Contrast to having deep pockets like kinase enzymes, a large surface areas and shallow interacting sites are observed in PPI working surface. Complicated signaling pathways involve multiple connectivity through some key points. These key points, known as hot-spots, contribute to the most binding energy of the complex. Development of peptides and small molecules that interact with hot-spots tend to exhibit high-affinity and selectivity.[28] In order to obtain specific inhibitors targeting Hsp90-Cdc37 complex interface, hot-spots was analyzed to discover potential high affinity peptides, which may avoid the drawbacks of natural product. In PPI cases, high affinity and selectivity modulators are usually based on oligopeptide, a series of famous small molecule PPI modulators

RSC Advances Accepted Manuscript

became successful starting from oligopeptides with moderate binding affinity.

In order to explore the hot-spots of the Hsp90-Cdc37 PPI interface, we presented a work flow (Fig. 1) based on molecular dynamics (MD) calculation. Molecular mechanics/poisson-boltzmann surface area (MM-PBSA) binding energy and energy decomposition scheme were combined to give the quantitative per-residue contribution for binding which revealed hot-spots Arg167 as a most important binding determinant. Following these implications, a series of Cdc37-derived peptides were designed and evaluated. An eleven-residue peptide (**Pep-1**), which exhibited the most potency, was identified and confirmed by isothermal titration calorimetry (ITC) and biolayer interferometry (BLI) assays to show low micromolar binding affinity (6.9 ± 0.9 μM) to Hsp90-Cdc37 PPI in a competitive manner. Subsequent detailed binding analysis of **Pep-1** was performed comparing with the structure of Hsp90-Cdc37 (2K5B). Binding mode of **Pep-1** to Hsp90-Cdc37 complex by molecular docking revealed that it not only occupied the Cdc37 binding site but also disrupted the ATP binding of Hsp90. The result was supported by ATPase inhibition assay ($IC_{50} = 3.0 \pm 0.07$ μM). **Pep-1** is the first small peptide that directly disrupts Hsp90-Cdc37 PPI. It provides a starting point for further structural simplification and optimization. The hot-spots we revealed may lead to the breakthrough in identifying small molecule inhibitors targeting Hsp90-Cdc37 PPI.
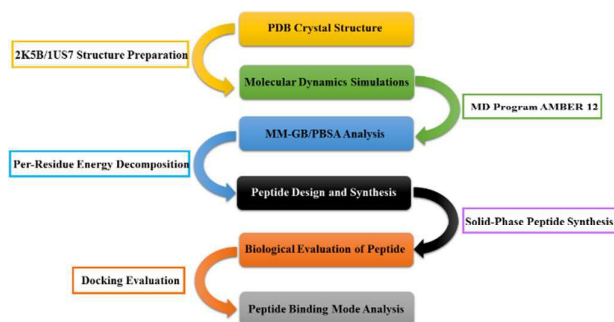
Fig. 1 Workflow of peptide discovery from computational start to biological evaluation

2. Materials and methods

2.1 Computational Methods

2.1.1 Protein preparation

The NMR structure (2K5B) and crystal structure (1US7) of Hsp90-Cdc37 complex were obtained from protein data bank (PDB). Clean protein tool in Discovery Studio (DS) 3.0 package (Accelrys Inc., San Diego, CA, USA) was used to correct the structure. Crystallographic water molecules were removed from the coordinate set. All calculations were conducted using Dawning TC2600 cluster.

2.1.2 MD Simulations

MD simulations of 2K5B and 1US7 was performed by PMEMD module of AMBER 12 program. The ff99SB force

field was applied to the complex.[29-31] TIP3P water molecules were utilized to solvate the complex, extending at least 10 Å from the protein. System was kept neutral by adding counterions. Before MD simulation, two steps of minimization were applied to the system. Firstly, the water molecules were refined through 2,500 steps of steepest descent followed by 2,500 steps of conjugate gradient, keeping the protein fixed with a constraint of 2.0 kcal mol^{-1} Å. Secondly, the complex was relaxed by 10,000 cycles of minimization procedure which contained 5,000 cycles of steepest descent and 5,000 cycles of conjugate gradient minimization. During the simulation, the particle mesh Ewald (PME) method was employed to calculate the long-range electrostatic interaction. SHAKE method was applied to constrain all covalent bonds involving hydrogen atoms to allow the time step of 2 fs. The whole system was heated from 0 to 300K running 50 ps molecular dynamics with position restraints under constant volume. 500 ps of the isothermal isobaric ensemble (NPT)-MD was conducted to adjust the solvent density for pressure relaxation with a time constant of 1.0 ps. In this step, all protein atoms were restraint by force constants of 2 kcal mol^{-1} Å Harmonic restraints. To relax the system without constraints, an extra 500 ps of unconstrained NPT-MD at 300K with a time a constant of 2.0 ps was performed. Finally, a length of 10 ns production dynamics at constant pressure was obtained. Snapshots of the trajectory were saved at 20 ps intervals for further analysis.

2.1.3 Analysis of MD trajectories and binding energy calculation

In order to explore the stability of the complex, the time-dependence of the RMSD of the backbone atoms was analyzed by 'ptraj' tool in AMBER12. Free energy calculation was performed by the MM-PBSA method. For MM-PBSA analysis, snapshots at 20 ps intervals were extracted from the 10 ns of the MD trajectory. The binding energy was averaged over the ensemble of conformers. MM-PBSA energy decomposition was conducted to explore the hot-spots residues.[32] In this procedure, the effective binding energies were decomposed into contributions of individual residues.

2.1.4 Docking

The Libdock tool in DS 3.0 was utilized to evaluate the designed small peptide. Peptide and protein were prepared using prepare ligands and prepare protein tool before docking. The docking site was derived from Cdc37 binding site of Hsp90 in crystal structure. The docking results were evaluated through comparison of the best docked poses. The RMSD was used to compare differences between the docked poses and the real crystal structure to measure docking reliability.

2.2 Peptide synthesis and protein purification

2.2.1 Chemical synthesis of peptide

300mg of 0.1mM Fmoc-Asp (OtBu)-RinkAmid MBHA Resin (sub = 0.33) was poured into a 250mL composite column, then DMF was added to swell for 3 hours. After DBLK solution was added, the whole system was performed under the protection of nitrogen for 30 minutes. Afterwards, DBLK solution was filtrated off and the filter cake was washed by DMF for 6 times. Three equivalents of amino acid and HBTU were added into the composite column and double resin volume of DMF was added subsequently. In addition, three equivalents of N-methyl morpholine was added before the reaction began. The endpoint was determined by negative ninhydrin reaction. The amino acids coupling liquid was filtered off and the resin was washed with DMF for 6 times and methanol for 3 times after the reaction finished. Deprotection was applied for all amino acids in

turns and then sealed N-terminal amino by acetic acid sealing solution (DMF: acetic oxide: N-methyl morpholine = 87: 6: 7). 600mg peptide-resin was obtained. 15mL lysis buffer (TFA: TIS: H2O = 95: 2.5: 2.5) was added into a round-bottom flask containing the peptide resin. The reaction was performed in the dark for 3 hours under the protection of nitrogen. Then the solution and resin were separated by sand core filtration and the resin was washed by TFA. The filtrate was poured into cold ether and centrifuged for precipitation. Then the crude product was precipitated with diethyl ether followed by HPLC purification using a C18 reversed phase column. Purity of the final peptides were analyzed by RP-HPLC and the characterization of the peptides was evaluated by electrospray ionization mass spectroscopy (ESI-MS). Detailed information was performed in Supporting Information.

2.2.2 Expression and purification of Hsp90N and Cdc37M

The region encoding N-terminal Hsp90 and Middle-domain Cdc37 were cloned into pET28a separately. 0.5 mM IPTG was used to induce the protein expression in *E. coli* cells. After 12 h growth at 17 °C, *E. coli* cells were harvested and sonicated. Then the clarified liquid solution was obtained by centrifugation. AKTA-pure (GE healthcare) was utilized to purify the soluble lysate. Equilibration buffer contained 25 mM Tris-Cl, 150 mM NaCl while elution buffer was consisted of 50 mM Tris-Cl and 10 mM reduced glutathione. Hsp90N and Cdc37M was identified by SDS-PAGE and dialyzed in 20% 0.1 mM PBS buffer, stored at -80 °C.

2.3 Biological Evaluation

2.3.1 Isothermal Titration Calorimetry (ITC)

An ITC200 calorimeter (Malvern) was used to carry out the ITC experiment. 300 μL of purified Hsp90N was fulfilled into the sample cell at a concentration of 100 μM in 0.01M PBS, pH 7.4. The syringe was filled with peptide in the same buffer condition. Two microliter aliquots of a 1 mM solution was titrated into the sample cell at 25 °C. 180 s intervals and a stirring speed of 1000 rpm were used for the whole procedure of the injection. In addition, a first 0.5 μL of ligand solution was titrated to prevent from initial interfering. All the data obtained from the experiment including association constant ($K_a = 1/K_d$), enthalpy value (ΔH) and entropy value (ΔS) were analyzed by the Origin software package.

2.3.2 Biolayer Interferometry (BLI)

The interaction between the peptide and the Hsp90 N-terminal protein was determined by biolayer interferometry using an OctetRed 96 instrument (ForteBio Inc.). Aminopropylsilane (APS) biosensors tips (ForteBio Inc., Menlo Park, CA) were selected to carry out the experiment. Before the protein was immobilized onto the APS biosensors, all the tips were placed in the buffer of 0.1 M PBS. Then the experiments were performed by following steps: (1) baseline. Sensors immersed in the 0.1M PBS buffer for 120 s to obtain equilibration; (2) protein loading to sensors. Sensor tips moved to Hsp90N protein plates to make protein immobilized for 600 s; (3) second baseline. Sensors moved to plates contained 0.1M PBST for 120 s to reach equilibration; (4) association. Sensors moved to ligand buffer for 300 s to obtain K_{on}; (5) dissociation. Sensors moved to 0.1 M PBST buffer for 300 s to obtain K_{off}. Four concentrations of ligands were utilized to obtain the final curve. All the data were analyzed by ForteBio data analysis software. Equilibrium dissociation constant (K_D) were carried out by the equation ($K_D = K_{off}/ K_{on}$).

2.3.3 Pep-1 competitive binding experiment

To characterize the disruption of Hsp90-Cdc37 complex by **Pep-1**, BLI assay was utilized. In this section, protein Cdc37 was immobilized onto the APS sensors. Positive control was performed using pure Hsp90N with a constant concentration 4 μM. Reference control contained only 0.1 M PBST buffer. Different concentrations of **Pep-1** (ranging from 20 μM to 2.2 μM with three times dilution) were mixed with Hsp90N (constant concentration 4 μM) to give a dose-dependent inhibition in a competitive manner. The experiment procedures were same as 2.3.2.

2.3.4 Hsp90 ATP Hydrolysis Assay

Following the instructions of the Discover RX ADP Hunter[TM] Plus Assay Kit (Discovery, Fremont. CA), the ATPase reactions were performed at 37 °C. Different concentrations of Cdc37-derived peptides and positive compound **AT13387** were tested in 384-well black plate. Varioskan multimode microplate spectrophotometer (Thermo Scientific Varioskan Flash, 540 nm excitation and 620 nm emission) was used to determine the ADP generation. Background value was measured in a solution lacking protein and ligand, while negative control was determined in a reaction lacking ligand and recognized as 100 % protein activity.

3. Results and discussion

3.1 MD Simulations and MM-PBSA calculation.

In order to explore the hot-spots of the Hsp90-Cdc37 complex binding interface, we applied a systematic peptide discovery workflow based on MD Simulations. After the crystal structure (PDB ID: 2K5B, 1US7) was prepared, long-range simulation trajectory (10 ns) was obtained for further binding energy calculation and per-residue decomposition analysis. System stability was examined through the RMSD of backbone atoms with respect to the structures obtained at the end of the production procedure (Fig. 2). According to the RMSD analysis, it was observed that 2K5B was more stable than 1US7 during the long-range trajectory, which demonstrated that the results of 2K5B might be more suitable for further analysis. It has been reported that MM-PBSA exhibited better in calculating the absolute binding free energies while MM-GBSA performed better in calculating relative binding free energies.[33] Through the binding free energy analysis, we expected to focus on the main driving force for the complex binding. Thus the MM-PBSA method was chosen to calculate the absolute binding free energies. Overall, the calculation results exhibited negative values of the complex effective binding energies, indicating a favorable PPI case. As shown in Fig. 2, 2K5B energy decomposition exhibited that nonpolar contribution were the major part of the total binding energy, indicating a large hydrophobic surface in Hsp90-Cdc37 binding. However, due to the large contact surface of the Hsp90-Cdc37 complex, the desolvation penalties (EPB) associated with the binding was huge which made the total electrostatic contribution of binding unfavorable. Finally, the ΔG_{total} was calculated as -5.4965 kcal/mol by the equation. ($\Delta G_{total} = \Delta G_{gas} + \Delta G_{solv}$)

A

B

RMSD
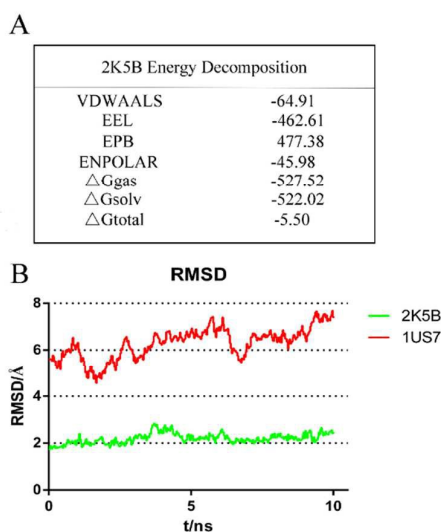
Fig. 2 MD simulation results. (A) 2K5B energy decomposition analysis. Mean energies are in kcal/mol, calculated from trajectory range 0-10 ns. VDWAALS = van der Waals contribution from MM. EEL = electrostatic energy as calculated by the MM force field. EPB = the electrostatic contribution to the solvation free energy calculated by PB. ENPOLAR = nonpolar contribution to the solvation free energy calculated by an empirical model. $\Delta G_{total} = \Delta G_{gas} + \Delta G_{solv}$. (B) Stability analysis for MD simulations. RMSD of 1US7 is shown in red while 2K5B shown in green.

3.2 Hot-spots identification for Hsp90-Cdc37 PPI

The per-residue contribution to the effective binding energy of the Cdc37 are listed in the Table 1. According to the per-residue decomposition of Cdc37 binding interface, it has been recognized that Lys160, His161, Met164, Leu165, Arg166 and Arg167 might contribute to the most binding free energy of the complex. Especially Arg167 (ΔG_{total} = -2.50 kcal/mol) contributes to nearly half of the complex binding energy which is consistent with the previously reported mutation results.[34] This result indicated that polar interactions such as hydrogen bond and salt bridge mediated by Arg167 may be one of the determinant for Hsp90-Cdc37 binding, therefore, Arg167 could be recognized as one of the most important hot-spots. In the case of Lys160, His161 and Arg166, though their ΔG_{total} are less than Arg167, electrostatic interactions of them are huge as well. According to the results, a series of peptides including all the residues mentioned above, was designed and synthesized to examine their binding capacity to Hsp90. Besides, peptides containing potential key residue mutations (R166A, R167A) were also designed and evaluated to determine the results from the hot-spots identification.

Table 1 Per-residue energy decomposition by MM-PBSA

Residues	Per-residue energy decomposition (kcal mol^{-1})			
	Van der waals	electrostatic	Polar solvation	total
Lys160	-0.06	-23.07	22.86	-0.27
His161	-0.19	-22.43	21.84	-0.78
Phe162	-0.03	-0.02	0.02	-0.03
Gly163	-0.04	-0.11	0.10	-0.05
Met164	-0.82	-0.22	0.83	-0.21
Leu165	-0.52	-0.23	0.35	-0.42
Arg166	-0.78	-20.83	20.86	-0.75
Arg167	-0.65	-23.15	21.30	-2.50
Trp168	-0.04	-0.08	0.08	-0.04
Asp169	-0.09	16.25	-16.13	0.04
Asp170	-0.26	16.87	-16.15	0.46

3.3 Cdc37-derived peptides bound to Hsp90N and inhibited Hsp90 ATPase

In order to determine the binding capacity of the peptides, ITC was applied to evaluate thermodynamics properties of the binding interaction. It was observed that **Pep-1** exhibited a huge energy release for the first three injections (about 9.0 μcal·s^{-1}) while bound to Hsp90N, indicating a favorable binding course. According to the curve-fitting analysis, a reversible 1:1 binding stoichiometry was obtained, hence it was demonstrated that one peptide molecule bound to one molecule of Hsp90N. Through all the parameters obtained, **Pep-1** exhibited the binding affinity with K_d of 6.9 μM to Hsp90N. Many researches have demonstrated that enthalpy of ligand binding (ΔH), which is composed of polar interactions such as hydrogen bonds, salt bridges and van der Waals energy, might play a significant role in specific binding.[35] While entropy-driven binding force (ΔS) mainly aimed at lipophilic interactions.[36] It is beneficial that a large negative value of ΔH might reflect a favorable force for non-covalent interactions changing from the free-state to the bound state. It is unfavorable to achieve large negative value of $-T\Delta S$ for a certain compound because it might result in nonspecific hydrophobic interactions, leading to poor target selectivity.[37] According to the ITC results, a favorable enthalpy component to binding (ΔH = -18.93 kcal/mol) and a moderate entropy ($-T\Delta S$ = 12.90 kcal/mol) were observed which illustrated hydrophilic contacts might be a determinant contribution to the binding. Hydrophobic interactions derived from entropy contribution might be an unfavorable driven force for complex binding while enthalpy contribution of specific binding interaction might be the determinants of the Hsp90-Cdc37 complex binding. Finally, the results of ΔG_{total} (-5.5 kcal/mol) calculated from MM-PBSA had a commendable coherence with the peptide binding results determined by ITC (ΔG = -7.0 kcal/mol) which illustrated that **Pep-1** contributed to the most binding energy of Cdc37.

Table 2 Cdc37-derived peptides binding capacity and inhibition rate of Hsp90 ATPase

Pep	Sequence	N	K_d (μM)	ΔG (kcal·mol^{-1})	IC$_{50}$ (μM) ATPase inhibition
1	Ac-KHFGMLRRWDD-NH$_2$	0.9 ± 0.3	6. 90 ± 0.9	-7. 00 ± 0.1	3.0 ± 0.1
2	Ac-KHFGMLRRWD-NH$_2$	1.0 ± 0.2	21.00 ± 2.8	-5.59 ± 0.2	4.8 ± 0.9
3	Ac-KHFGMLRRW-NH$_2$	0.8 ± 0.2	10.07 ± 1.9	-6.37 ± 0.2	3.7 ± 0.7
4	Ac-FGMLRRWDD-NH$_2$	1.1 ± 0.1	15.62 ± 1.8	-6.50 ± 0.2	36.9 ± 3.3
5	Ac-MLRRWDD-NH$_2$	1.1 ± 0.3	18.55 ± 3.9	-6.47 ± 0.3	45.8 ± 2.7
6	Ac-MLRR-NH$_2$	N/A^a	N/A^a	N/A^a	N/A^a
7-mut	Ac-KHFGMLRAWDD-NH$_2$	1.1 ± 0.4	518.1 ± 7.9	-4.50 ± 0.4	> 100
8-mut	Ac-KHFGMLARWDD-NH$_2$	1.3 ± 0.2	114.3 ± 6.4	-5.42 ± 0.3	> 100

^{a} No Activity

To determine the effectiveness of **Pep-1** binding affinity results and make furthersome compare, more Cdc37-derived peptides were designed and synthesized (Table 2). All of them were evaluated by ITC and Hsp90 ATPase inhibition assay (Table 2). **Pep-2** and **Pep-3** were used to explore the function of Asp169 and Asp170 in C-terminal of the **Pep-1**, which exhibited a two to three times binding affinity loss (**Pep-2:** 21.00 ± 2.8 μM, **Pep-3:** 10.07 ± 1.9 μM) compared with **Pep-1** (6. 90 ± 0.9 μM). While ATPase inhibition ability (**Pep-2:** 4.8 ± 0.9 μM, **Pep-3:** 3.7 ± 0.7 μM) was not seriously affected by the reduction of Asp169 and Asp170. **Pep-4** and **Pep-5** were utilized to test the effectiveness of Lys160, His161, Phe162 and Gly163, which showed a nearly three times binding affinity loss (**Pep-4:** 15.62 ± 1.8 μM, **Pep-5:** 18.55 ± 3.9 μM) and ten times ATPase inhibition ability loss (**Pep-4:** 36.9 ± 3.3 μM, **Pep-5:** 45.8 ± 2.7 μM). With the decrease of binding affinity, ΔG dropped as well. **Pep-6** only contained four potential key residues (Met164, Leu165, Arg166 and Arg167) had lost its binding capacity and ATPase inhibition ability totally. These results illustrated that Lys160, His161, Phe162 and Gly163 might have a huge effect on ATPase inhibition while Asp169 and Asp170 might have a slightly contribution to **Pep-1** binding capacity. Potential key residues Arg166 and Arg167 were mutated to obtain **Pep-7-mut** and **Pep-8-mut**. Both of them exhibited a significant binding affinity loss, especially mutation of R167A, and ATPase inhibition ability loss. This results

commendably proved the Hot-spots and key residue of Arg167 we mentioned above.

In order to demonstrate the effectiveness of **Pep-1**, the BLI assay was utilized to determine its binding capacity. BLI is one of the most common ways to quantify the binding affinity of peptide-protein interaction.[38] The measured K_D value of **Pep-1** was 6.01 μM with proper fitting curves. A dose-dependently inhibitory manner was also observed according to the curves. Both K_{on} and K_{off} value show tolerant extent for peptide-protein binding. K_D value was calculated as following equation: $K_D = K_{off} / K_{on}$. This is the first evidence that a small peptide derived from co-chaperone protein can effectively bind to Hsp90.

Hsp90 ATPase inhibition determination by Cdc37-derived peptides was performed using an assay of Discover RX ADP Hunter^{TM} Plus Assay Kit The final data showed that **Pep-1** inhibited Hsp90 ATPase with IC$_{50}$ 3.0 ± 0.07 μM by a dose-dependent manner. Meanwhile, **AT13387** was used as positive control giving IC$_{50}$ 0.5 ± 0.15 μM. All the data was shown in Table 2. This result kindly proved our following binding mode. **Pep-1** showed a moderate activity of Hsp90 ATPase inhibition compared with the positive control AT13387. In addition, **Pep-1** might locate on Hsp90 ATPase site nearby and interfere with Cdc37 binding to Hsp90 through an allosteric regulation.
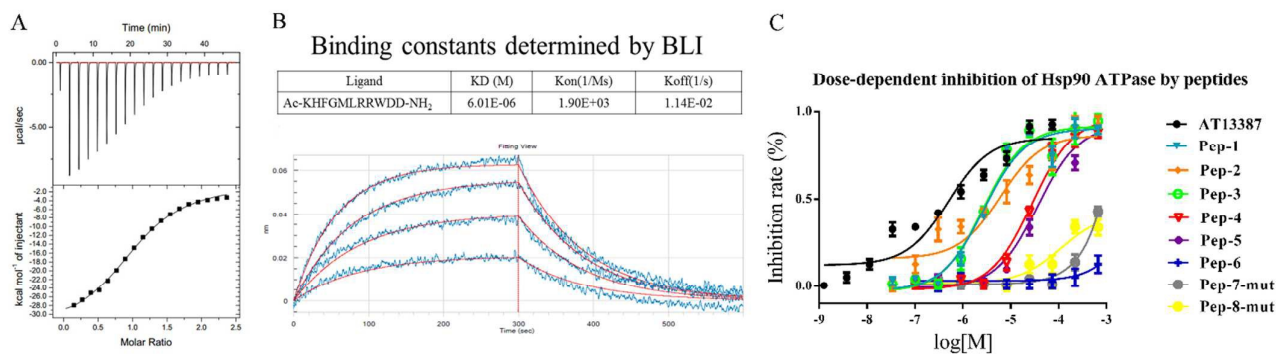
Fig. 3 (A) The ITC fitting curve clearly fits a 1 : 1 reversible binding mode with a K_d of 6.7 μM. (B) BLI dose-response curves of the **Pep-1** reflecting the direct binding to Hsp90N. Concentrations ranged from 3.2 μM to 0.0256 μM with 5 times dilution of each curve. (C) Dose dependent inhibition of Hsp90 ATPase by peptides.
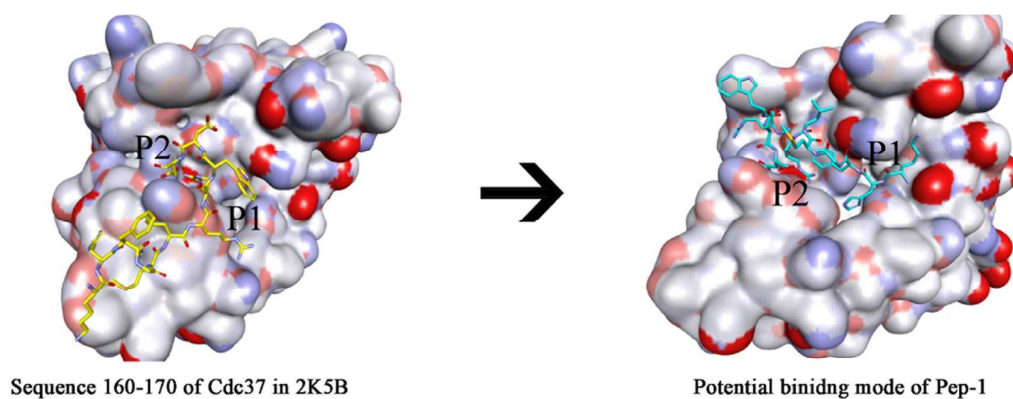
Fig .4 Potential binding mode analysis of **Pep-1**. Structure of Hsp90-Cdc37 complex (Cdc37 only exhibited sequence 160-170) compared with potential binding mode of **Pep-1**, P1 is ATP binding pocket. P2 is potential Cdc37 binding cleft.

3.4 Potential binding mode of the Pep-1

Hsp90-Cdc37 PPI is a case with moderate binding affinity probably because there is no obvious and deep cavity in both Hsp90 and Cdc37 binding interface. The structure of Hsp90-Cdc37 formed through several key residues, Arg167 of Cdc37 and Glu47 of Hsp90 are considered to be one of the most important interactions. It has been reported that the side chain of Arg167 could insert into the mouth of ATPase nucleotide binding pocket, forming significant hydrogen bond with Glu47 of Hsp90N, to moderately interfere with ATPase ability of Hsp90.[39] However, according to the cocrystal structure of Hsp90-Cdc37 (Fig. 4 left), Arg167 can not insert deeply into P1 to bind tightly with Hsp90, this could be one of the reasons that Cdc37 can not effectively inhibit the ATPase of Hsp90N. However, our results showed that **Pep-1** can not only bind to Hsp90, but also inhibit the ATPase activity of Hsp90N. Therefore, we inferred that **Pep-1** might form different binding mode to Cdc37 when bound to Hsp90N. To explain the result, molecular docking was performed to analyze the binding mode of Hsp90N-**Pep-1**. Compared to Cdc37, **Pep-1** had improved structural flexibility to form different binding mode and orientation in the groove of Hsp90N, leading to a simultaneous occupation of P1 and P2 of Hsp90N (Fig.4, right). P1 is occupied by residue Lys160 and His161 of **Pep-1**, which deeply inserted into the ATP binding pocket of Hsp90N. The mode indicated that the two residues were important for the activity of **Pep-1**. The results were consistent with the per-residue decomposition analysis mentioned above (contributed nearly 20% to complex binding). P2 of Hsp90N was well occupied by Met164, Leu165, Arg166 and Arg167 of **Pep-1**, supplying the main binding affinity to Hsp90N.

3.5 Pep-1 interfered with Hsp90-Cdc37 PPI

To characterize the disruption of Hsp90-Cdc37 complex by **Pep-1**, BLI assay was utilized. In this section, protein Cdc37 was loaded onto the sensors. Different plates (one fulfilled with protein Hsp90N, others included Hsp90N and **Pep-1** mixture) were used simultaneously to evaluate the binding capacity of Hsp90N. Red curve represents the direct binding of Cdc37 to

Hsp90N while others stands for Cdc37 binding to the mixture of Hsp90N and **Pep-1** (Hsp90N stays in the constant concentration, 4 μM, in all plates). **Pep-1** concentrations changed from 20 μM to 2.2 μM with three times dilution. It is obvious that after **Pep-1** was added, the binding capacity of Hsp90N decreased a lot. The signal declined following dose-dependent of the **Pep-1**. This results illustrate that Hsp90-Cdc37 binding complex might be interfered by **Pep-1**.
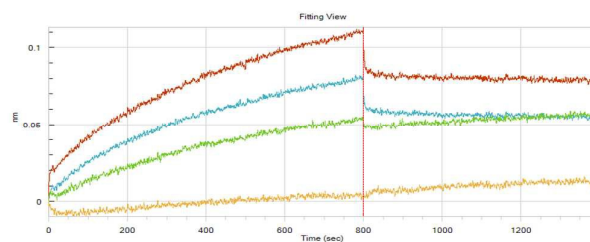
Fig. 5 BLI association and disassociation curves in two different conditions. Red curve stands for Cdc37 directly binding to Hsp90. Other curves stand for Cdc37 binding to the mixture of Hsp90 and **Pep-1**. Hsp90 was kept in constant concentration at 4 μM while concentration of **Pep-1** ranging from 20 μM to 2.2 μM with three times dilution. (**Pep-1** concentration: red curve 0 μM, sky blue curve 2.2 μM, green curve 6.7 μM, orange curve 20 μM). A significant signal decline could be obtained after different concentrations of **Pep-1** was added. It is obvious that with rising concentrations of the **Pep-1**, the Hsp90 binding signal decreased. All the groups were performed with 800s association part and 600s dissociation part.

4. Discussions

Although there are several co-crystal structures of Hsp90-Cdc37 PPI reported, it is still not clear that which region of Cdc37 is the most important part for its binding to Hsp90. The affinity of Hsp90-Cdc37 complex is at low μM which make it more difficult to discover disruptors beginning with peptide. Taking a briefly observation of the Hsp90-Cdc37 binding interface, a loop-region (sequence 160-170) and a very short helix (sequence 200-210) of Cdc37 were reported being significant for Hsp90-Cdc37 complex binding. However, these two parts were far away from each other, making the whole binding interface of the complex very large, thus it is very difficult to design small molecule inhibitor without revealing

ARTICLE

the hotspots of this PPI. According to the crystal structure of the complex, the loop-region (sequence 160-170) of Cdc37 might be more likely to become peptide inhibitors comparing with the short helix (sequence 200-210), because it might occupy the deep-long cavity of Hsp90 next to ATP pocket. By comparison, it seems that the short helix only binds to a shallow and narrow groove, which cannot supplies stable binding pocket for Hsp90-Cdc37 PPI. To reveal which part contains important hotspots for this PPI, in this study, molecular dynamics simulation accompanied by MM-PBSA analysis, which is commonly used to evaluate the binding free energy of PPI interface and identify hotspots of the intermolecular interaction, is applied to achieve our goal. According to the results, the loop part, especially Arg166 and Arg167, contribute the most binding energy to the PPI, therefore, they can be recognized as the hotspots of Hsp90-Cdc37 interaction.

Discovering highly efficient modulators targeting PPI is one of the most challenge task in medicinal chemistry. The large binding domain make it very difficult to design the modulators directly from small molecules. From this point of view, an active oligopeptide can provide ideal template to reveal the chemical space of the PPI and guide the compound design, because it can not only occupy the binding interface to the utmost, but also provide a scaffold which is easily to be modified to obtain druggable small molecules. Therefore, an active oligopeptide targeting the PPI is urgently needed to act as the starting point of the research. Actually, many successful inhibitors targeting PPI are initiated from the discovery of peptides with moderate activity, such as AT-406 in XIAP,[40] MI-888 in MDM2-P53,[41] MM-410 in MLL1-WRD5,[42] MCP-1 in MLL1-Menin.[43]

Although it is a common strategy to discover potent peptides directly from PPI binding interface, different PPI cases have different challenges. Most of the initial PPI oligopeptides were derived from the alpha-helix part at the binding interface of the two proteins. Short peptides were designed to maintain the conformation of alpha-helix which containing potential key residues on PPI binding interface. It is easier to obtain higher affinity because of the settled conformation and deep interaction cavity. While in the case of Hsp90-Cdc37, the binding interface is shallow and flat, no stable and typical alpha-helix was observed at the binding interface. Instead, a loop region comprised of residues 160-170 of Cdc37, is most likely to occupy the cleft next to the ATP pocket in Hsp90. In such condition, it is more difficult to discover active peptides compared to the cases that the alpha-helix acts as the binding part, because loop region is highly flexible without stable conformation, it is not easy to know which residues act as hotspots.

Pep-1, which directly binds to Hsp90 with K_d in low micromolar range and blocks Cdc37-Hsp90 PPI, has provided us a good template for designing small molecule inhibitor of Cdc37-Hsp90 PPI. Although previously some natural products, such as celastrol, have been inferred to affect Cdc37-Hsp90 PPI, the target selectivity as well as the activity are not satisfactory. Besides, it is hard to chemically modify the scaffold of these complicated natural product. **Pep-1**, however, is directly obtained from Cdc37, it can act as a more ideal template to design of small molecule inhibitor directly targeting Hsp90-Cdc37 PPI. Therefore, it can serve as the starting point for further structural optimization.

5. Conclusions

In summary, a combined strategy of MD simulation and MM-PBSA analysis was performed to give a quantitative per-residue contribution. Based on the calculation results and whole binding interface observation as well as interaction properties, Cdc37-derived peptides were designed and synthesized. ITC

and BLI assays were carried out to evaluate the binding capacity of peptides which revealed **Pep-1** with highest binding affinity and ATPase inhibition ability. **Pep-1** is the first evidence that a non-natural inhibitor could bind to Hsp90 not only inhibit the ATPase ability but also disrupt Cdc37 binding. In this study, the combined strategy of molecular dynamic simulation and MM-PBSA approach showed its value in exploring the PPI binding interface as well as peptide design. Further studies may focus on the effectiveness of the peptide to reveal the key residues and the minimized sequence of the potent peptide.

Acknowledgements

Notes and references

1   G. Chiosis, C. A. Dickey and J. L. Johnson, *Nat. Struct. Mol. Biol.*, 2013, **20**, 1-4.
2   M. A. Biamonte, R. Van de Water, J. W. Arndt, R. H. Scannevin, D. Perret and W. C. Lee, *J. Med. Chem.*, 2010, **53**, 3-17.
3   J. R. Porter, C. C. Fritz and K. M. Depew, *Curr. Opin. Chem. Biol.*, 2010, **14**, 412-420.
4   S. K. Calderwood, *Scientifica (Cairo)*, 2013, 217513.
5   S. K. Calderwood, *Subcell. Biochem.*, 2015, **78**, 103-112.
6   S. Polier, R. S. Samant, P. A. Clarke, P. Workman, C. Prodromou and L. H. Pearl, *Nat. Chem. Biol.*, 2013, **9**, 307-312.
7   A. Ota, J. Zhang, P. Ping, J. Han and Y. Wang, *Circ. Res.*, 2010, **106**, 1404-1412.
8   Y. Wang, W. Xu, D. Zhou, L. Neckers and S. Chen, *J. Biol. Chem.*, 2014, **289**, 4815-4826.
9   C. M. Gould, N. Kannan, S. S. Taylor and A. C. Newton, *J. Biol. Chem.*, 2009, **284**, 4921-4935.
10 A. Marino-Enriiquez, W. B. Ou, G. Cowley, B. Luo, A. H. Jonker, M. Mayeda, M. Okamoto, G. Eilers, J. T. Czaplinski, E. Sicinska, Y. Wang, T. Taguchi, G. D. Demetri, D. E. Root and J. A. Fletcher, *Oncogene*, 2014, **33**, 1872-1876.
11 M. Hinz, M. Broemer, S. C. Arslan, A. Otto, E. C. Mueller, R. Dettmer and C. Scheidereit, *J. Biol. Chem.*, 2007, **282**, 32311-32319.
12 F. Y. Wu, S. O. Peacock, S. Y. Rao, S. K. Lemmon and K. L. Burnstein, *J. Biol. Chem.*, 2013, **288**, 5463-5474.
13 C. K. Vaughan, U. Gohlke, F. Sobott, V. M. Good, M. M. U. Ali, C. Prodromou, C. V. Robinson, H. R. Saibil and L. H. Pearl, *Mol. Cell*, 2006, **23**, 697-707.
14 T. Erazo, A. Moreno, G. Ruiz-Babot, A. Rodriguez-Asiain, N. A. Morrice, J. Espadamala, J. R. Bayascas, N. Gomez and J. M. Lizcano, *Mol. Cell. Biol.*, 2013, **33**, 1671-1686.
15 S. Park, B. Dong and F. Matsumura, *Biochemistry*, 2007, **46**, 899-908.
16 A. Ota and Y. Wang, *J. Biol. Chem.*, 2012, **287**, 6266-6274.
17 T. Prince, L. Sun and R. L. Matts, *Biochemistry*, 2005, **44**, 15287-15295.
18 U. K. Jinwal, J. F. Abisambra, J. Zhang, S. Dharia, J. C. O'Leary, T. Patel, K. Braswell, T. Jani, J. E. Gestwicki and C. A. Dickey, *J. Biol. Chem.*, 2012, **287**, 24814-24820.

RSC Advances Accepted Manuscript

19 D. De Nardo, P. Masendycz, S. Ho, M. Cross, A. J. Fleetwood, E. C. Reynolds, J. A. Hamilton and G. M. Scholz, *J. Biol. Chem.*, 2005, **280**, 9813-9822.

20 U. K. Jinwal, J. H. Trotter, J. F. Abisambra, J. Koren, L. Y. Lawson, G. D. Vestal, J. C. O'Leary, A. G. Johnson, Y. Jin, J. R. Jones, Q. Y. Li, E. J. Weeber and C. A. Dickey, *J. Biol. Chem.*, 2011, **286**, 16976-16983.

21 A. D. Basso, D. B. Solit, G. Chiosis, B. Giri, P. Tsichlis and N. Rosen, *J. Biol. Chem.*, 2002, **277**, 39858-39866.

22 J. H. Joo, F. C. Dorsey, A. Joshi, K. M. Hennessy-Walters, K. L. Rose, K. McCastlain, J. Zhang, R. Iyengar, C. H. Jung, D. F. Suen, M. A. Steeves, C. Y. Yang, S. M. Prater, D. H. Kim, C. B. Thompson, R. J. Youle, P. A. Ney, J. L. Cleveland and M. Kundu, *Mol. Cell*, 2011, **43**, 572-585.

23 H. Gaude, N. Aznar, A. Delay, A. Bres, K. Buchet-Poyau, C. Caillat, A. Vigouroux, C. Rogon, A. Woods, J. M. Vanacker, J. Hohfeld, C. Perret, P. Meyer, M. Billaud and C. Forcet, *Oncogene*, 2012, **31**, 1582-1591.

24 J. R. Smith, P. A. Clarke, E. de Billy and P. Workman, *Oncogene*, 2009, **28**, 157-169.

25 T. Zhang, A. Hamza, X. Cao, B. Wang, S. Yu, C. G. Zhan and D. Sun, *Mol. Cancer Ther.*, 2008, **7**, 162-170.

26 T. Zhang, Y. Li, Y. Yu, P. Zou, Y. Jiang and D. Sun, *J. Biol. Chem.*, 2009, **284**, 35381-35389.

27 S. Sreeramulu, S. L. Gande, M. Gobel and H. Schwalbe, *Angew. Chem. Int. Ed. Engl.*, 2009, **48**, 5853-5855.

28 A. A. Bogan and K. S. Thorn, *J. Mol. Biol.*, 1998, **280**, 1-9.

29 E. Darian and P. M. Gannett, *J. Biomol. Struct. Dyn.*, 2005, **22**, 579-593.

30 V. Hornak, R. Abel, A. Okur, B. Strockbine, A. Roitberg and C. Simmerling, *Proteins*, 2006, **65**, 712-725.

31 C. Simmerling, B. Strockbine and A. E. Roitberg, *J. Am. Chem. Soc.*, 2002, **124**, 11258-11259.

32 H. Gohlke, C. Kiel and D. A. Case, *J. Mol. Biol.*, 2003, **330**, 891-913.

33 J. W. Tingjun Hou , Youyong Li , and Wei Wang, *J. Chem. Inf. Model.,*, 2011, **51**, 69–82.

34 Y. Jiang, D. Bernard, Y. Yu, Y. Xie, T. Zhang, Y. Li, J. P. Burnett, X. Fu, S. Wang and D. Sun, *J. Biol. Chem.*, 2010, **285**, 21023-21036.

35 M. Citartan, S. C. Gopinath, J. Tominaga and T. H. Tang, *Analyst*, 2013, **138**, 3576-3592.

36 E. Freire, *Drug Discov. Today*, 2008, **13**, 869-874.

37   T. S. G. Olsson, M. A. Williams, W. R. Pitt and J. E. Ladbury, *J. Mol. Biol.*, 2008, **384**, 1002-1017.

38   S. Geschwindner, J. Ulander and P. Johansson, *J. Med. Chem.*, 2015, DOI: 10.1021/jm501511f.

39 A. M. Roe SM1, Meyer P, Vaughan CK, Panaretou B, Piper PW, Prodromou C, Pearl LH., *Cell*, 2004, **116**, 87-98

40 J. F. DiPersio, H. P. Erba, R. A. Larson, S. M. Luger, M. S. Tallman, J. M. Brill, G. Vuagniaux, E. Rouits, J. M. Sorensen and C. Zanna, *Clin. Lymphoma Myeloma Leuk.*, 2015, **15**, 443-449.

41 Y. Zhao, S. Yu, W. Sun, L. Liu, J. Lu, D. McEachern, S. Shargary, D. Bernard, X. Li, T. Zhao, P. Zou, D. Sun and S. Wang, *J. Med. Chem.*, 2013, **56**, 5553-5561.

42 F. Cao, E. C. Townsend, H. Karatas, J. Xu, L. Li, S. Lee, L. Liu, Y. Chen, P. Ouillette, J. Zhu, J. L. Hess, P. Atadja, M. Lei, Z. S. Qin, S. Malek, S. Wang and Y. Dou, *Mol. Cell*, 2014, **53**, 247-261.

43 H. Zhou, L. Liu, J. Huang, D. Bernard, H. Karatas, A. Navarro, M. Lei and S. Wang, *J. Med. Chem.*, 2013, **56**, 1113-1123.